ACS Macro Letters

Letter

Cite This: ACS Macro Lett. 2018, 7, 1120−1125

pubs.acs.org/macroletters

Self-Coacervation of a Silk-Like Protein and Its Use As an Adhesive for Cellulosic Materials

Pezhman Mohammadi,*[,†] Grégory Beaune,[‡] Bjørn Torger Stokke,[§] Jaakko V. I. Timonen,[‡] and Markus B. Linder*[,†]

[†]Department of Bioproducts and Biosystems, School of Chemical Engineering, Aalto University, FI-02150, Espoo, Finland

[‡]Department of Applied Physics, School of Science, Aalto University, FI-02150, Espoo, Finland

[§]Biophysics and Medical Technology, Department of Physics, The Norwegian University of Science and Technology, NTNU, NO-7491 Trondheim, Norway

Supporting Information

ABSTRACT: Liquid−liquid phase separation of biomacromolecules plays a critical role in many of their functions, both as cellular components and in structural assembly. Phase separation is also a key mechanism in the assembly of engineered recombinant proteins for the general aim to build new materials with unique structures and properties. Here the phase separation process of an engineered protein with a block-architecture was studied. As a central block, we used a modified spider silk sequence, predicted to be unstructured. In each terminus, folded globular blocks were used. We studied the kinetics and mechanisms of phase formation and analyzed the evolving structures and their viscoelastic properties. Individual droplets were studied with a micropipette technique, showing both how properties vary between individual drops and explaining overall bulk rheological properties. A very low surface energy allowed easy deformation of droplets and led to efficient infiltration into cellulosic fiber networks. Based on these findings, we demonstrated an efficient use of the phase-separated material as an adhesive for cellulose. We also conclude that the condensed state is metastable, showing an ensemble of properties in individual droplets and that an understanding of protein phase behavior will lead to developing a wider use of proteins as structural polymers.

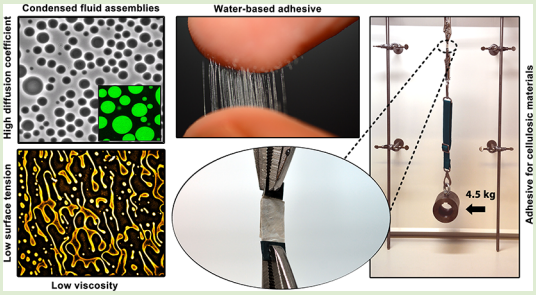

Some proteins show phase separation, leading to the formation of a condensed protein-rich phase and a phase depleted of protein. Such condensed phases are referred to as coacervates or condensates.[1] Protein phase separation is recognized in many biological systems to be either functionally important in cell biology[2] or as an intermediate step in the formation structural assemblies, such as adhesives[3] or in biomineralization.[4] The high concentration of protein and their increased interactions can also lead to undesired events such as pathological aggregates.[5] It is generally understood that the weak interactions that drive phase separation are important for subsequent assembly steps of biological functionality. The polymer behavior of proteins in these condensed phases is therefore of key importance for a fundamental understanding.

In many of the examples where condensation leads to materials, the condensation occurs with only one species of protein, such as squid-beak protein,[6] nacre,[4] and mussel[7] or sandcastle adhesives.[8] Such phase separation of a single component is often referred to as self-coacervation.[9] Often these proteins are intrinsically disordered.[10] While a high protein concentration and favorable preorganization is beneficial in fiber assembly, condensates also show additional advantages when functioning as adhesives. One is that condensates have a low surface energy that allows them to efficiently infiltrate porous structures and to wet their internal surfaces. Condensates that function extracellularly also prevent the dissolution of the adhesive into the environment, which is especially important in marine adhesives. The high protein concentration and their increased interactions can also lead to a rapid trigger of adhesion and curing.[3,8]

Here we describe the detailed characterization of spider silk (spidroin)-inspired protein coacervates and their use as adhesives for cellulosic materials. Applications involving cellulose are rapidly expanding due to its excellent structural and functional properties in combination with new ways to process and use it.[11] Consequently, new types of biological materials are expected. We noted previously that a block-architecture in which a spidroin repetitive sequence is flanked in both N and C termini by folded domains leads to a self-coacervating phase behavior[12] (Figures 1A and S1−S4). The general architecture was important for coacervation, and the same behavior was achieved even with other unrelated proteins used as terminal domains. The block design of the recombinant proteins was inspired by the structure of spidroins,[13] but it does not necessarily follow that the mechanisms described here apply for

Received: July 14, 2018
Accepted: August 29, 2018
Published: September 5, 2018

DOI: 10.1021/acsmacrolett.8b00527
ACS Macro Lett. 2018, 7, 1120−1125

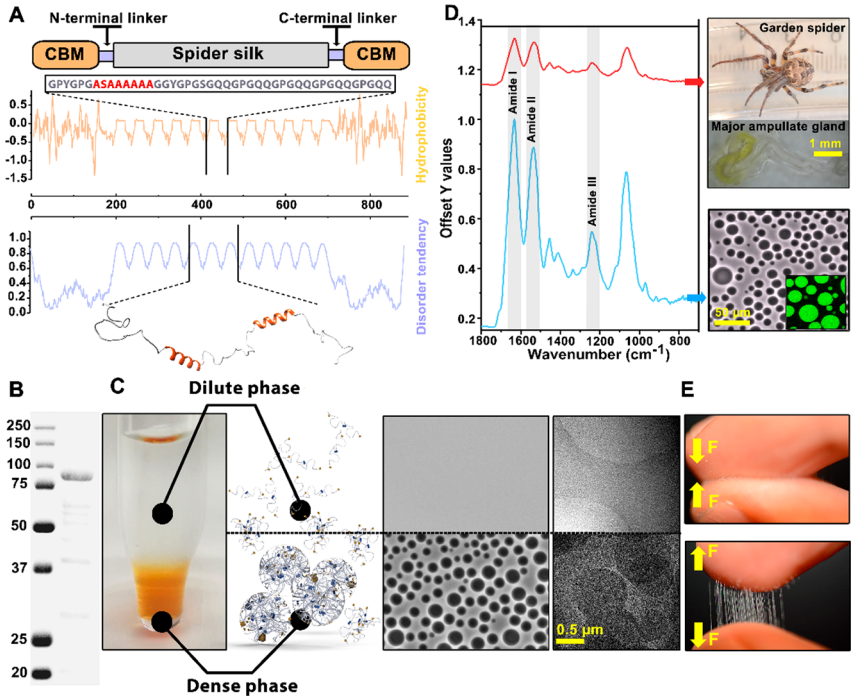

Figure 1. Self-coacervation of CBM-eADF3-CBM. (A) Schematic representation of the engineered CBM-eADF3-CBM fusion protein. Plots show hydrophobicity (Hopp and Wood scale) and disorder tendency profiles. (B) SDS-PAGE of CBM-eADF3-CBM. (C) Liquid–liquid phase separation of the CBM-eADF3-CBM in pure water. (D) ATR-FTIR spectra of 30% w/v LLC solution (blue line) and extracted natural spider silk solution (red line), showing similar signals in regions sensitive to secondary structure. (E) Pulling apart a drop of LLC between fingers results in the formation of continuous filaments and illustrates its viscoelastic and adhesive behavior.

native spidroins. The repetetitive spidroin sequence used here was an engineered version containing 12 repeats of residues 325−368 of the load-bearing repetitive major ampullate spidroin 3 from *Aaraneus diadematus* (eADF3).[14−16] The main feature in the primary structure of this protein is the repetition of short poly-A stretches flanked by P-, G-, and Q-rich stretches (Figure S5). This results in a sequence with alternating hydrophobic and hydrophilic properties[17] and a high predicted disorder tendency.[18] As terminal blocks, the structurally folded and thermally stable family 3 cellulose-binding module (CBM)[19] from the *Clostridium thermocellum* cellulosome were used. These blocks show a high affinity toward cellulose. Linkers between blocks were from the major ampullate spidroin 1 from *Euprosthenops australis*.[20]

Closer examination of the dense phase revealed that it consists of small droplets. To make a distinction to previously described phase separation that was achieved by adding potassium phosphate, we name the system under study here LLC (liquid-like coacervate (or condensate)).[12] The LLCs form spontaneously when protein concentration is a high and ionic strength is low. The LLC-containing phase remained stable at even 30% protein concentration. Interestingly, the ATR-FTIR spectra which is sensitive to secondary structure conformation showed similarity to dissected spider silk dope (Figure 1D). The LLC solution showed a high adhesiveness to surfaces and forming long filaments when pulled apart (Figure 1E).

To address the question of how LLC droplets formed and grew, we used spatial light interference microscopy (SLIM). With this interferometry-based method, dry mass can be measured in a microscope setup.[21] We observed how independent drops emerged in a previously mixed sample (Figure 2A, Videos 1 and 2 and Figure S6). The curves showing an increase in dry mass were obtained by identifying spots were droplets appeared and recording integrated mass content of that location in video replays. After droplet initiation, a linear region of growth occurred until a slow leveling of the growth rate. Droplets grew larger by coalescence with droplet fusions adding to dry mass in an additive way as expected (Figure 2B, Video 3). The ratio of dry mass in a droplet to dry mass of a droplet-free surrounding of the same size was calculated for a sample of 15 droplets and gave a ratio of 140 with a standard deviation (SD) of 51.

In a solution containing LLCs, the diffusivities of molecules in both the surroundings and within the LLCs were measured using fluorescence recovery after photobleaching (FRAP; Video 4). Proteins in the surroundings showed diffusion constants ranging from 2.3×10^{-7} cm^2 s^{-1} to 7×10^{-6} cm^2 s^{-1} (Figure 2C). The proteins within the coacervates moved much slower with diffusion constants from 1×10^{-9} cm^2 s^{-1} to 10×10^{-9} cm^2 s^{-1}. Probing droplets of different size showed significant variation in the diffusion rates (Figure 2C). Analyzing the internal structure of the condensed LLC droplets using cryo-fracturing and high-resolution SEM imaging (Figure 2D) showed that the proteins are internally assembled in an interconnected bicontinuous network.

Shear rate dependent viscosity measurements showed that a solution containing LLCs showed shear thinning with increasing shear rates. At the onset of shear, the LLC containing solution had a viscosity of 490 Pa·s (Figure 3A). However, above the critical shear rate of 0.002 s^{-1}, the solution showed shear thinning. At a shear rate of 0.87 s^{-1} the viscosity had dropped to 60 Pa·s. In an oscillatory shear stress test, LLC containing solutions showed a shear-induced gelation with gradual viscoelastic stiffening with $G' \gg G''$, that is, a dominant elastic response (Figure 3B).

DOI: 10.1021/acsmacrolett.8b00527
ACS Macro Lett. 2018, 7, 1120−1125

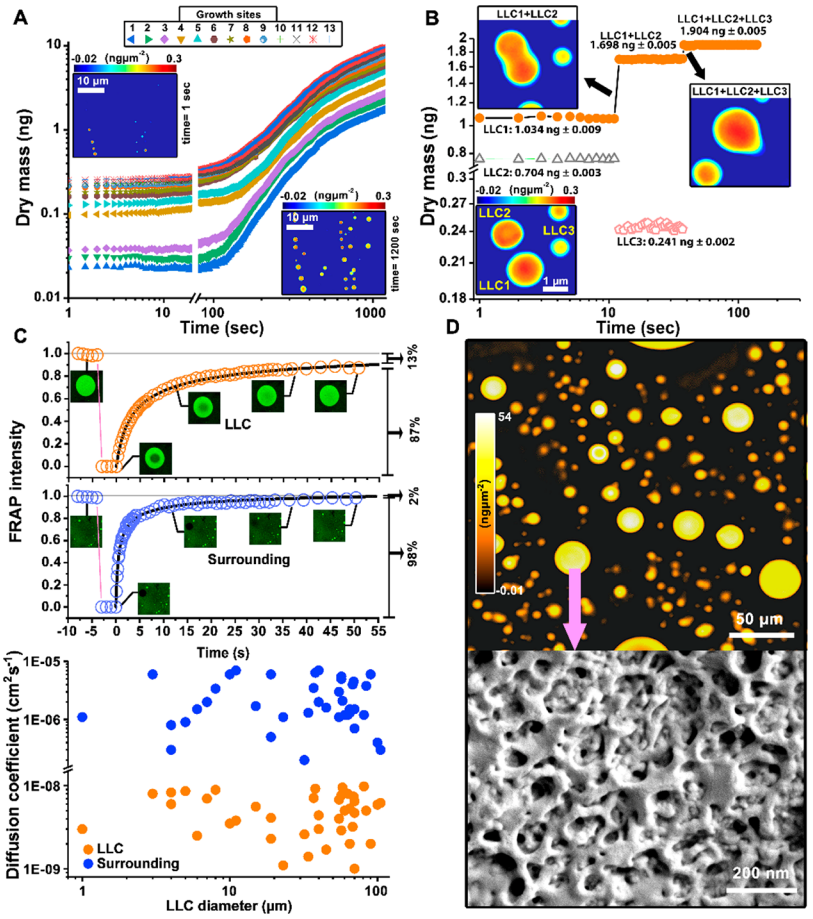

Figure 2. Formation and growth of LLC droplets. (A) Dry mass vs time for 13 LLC droplets that nucleated and grew at multiple sites. (B) Coalescence of three individual LLC droplets, each varying in size and protein content, resulting in an increase in the protein content of the main droplet after each fusion. (C) Recovery curves for the fluorescence signal after photobleaching of a LLC and its surrounding. (D) SLIM and SEM images of the LLC droplets. The SEM shows an internal bicontinuous structure.

However, as the bulk viscosity properties must be affected by the properties of the LLC droplets contained inside, an analysis of the properties of individual LLC droplets within the dilute phase was made. Measurements were made by aspiration with a micropipette submerged in the solution (Figure 3C, Video 4, Figures S7 and S8). In addition to viscosity, we could measure additional characteristics (Figure 4A), such as modulus and surface tension, by independent analysis in situ. The individual LLC droplets demonstrated viscoelastic properties. This was evident from the creep behavior in the aspiration and retraction curves (Figure S9), with an initial elastic regime which was followed by a linear viscous regime. Droplets had low viscosities ranging from 1 to 74 Pa·s, and Young's moduli ranging from 1.3 to 43 Pa. The surface tension was also very low, with values ranging from 7 to 76 μNm^{-1}. As with measurements of diffusion rates, there was a considerable range of values spanning an approximately 10-fold range for all parameters. However, all measured droplets had an overall very low interfacial energy and a high deformability. As expected from the combination of low surface energy and low viscosity, the LLC droplets were easily deformed during flow (Figure 4A and Video 6). Freezing a sample very quickly after deformation using liquid ethane and cryo-fracturing showed by SEM imaging how the internal bicontinuous structure deformed and elongated together with the droplet (Figure 4A) with compression and stretching of the bicontinuous structure, leading to a partial alignment of the network components.

The behavior of the droplets provides an understanding of the bulk rheology in general terms. The elongation of droplets during deformation is expected to lead to a shear thinning, as elongated drops slide more easily past each other. The observed shear-induced gelation with a high ratio of elastic modulus to loss modulus is likewise expected since elongated droplets are induced by shear. The elastic recovery is expected as elongated droplets regain their spherical shapes. Overall, the bulk properties are reminiscent of many previously described occurrences of coacervates, such as marine adhesives and in the formation processes of squid beaks.[6] In the squid beak formation, the combination of properties allows efficient impregnation and cross-linking of a chitin network. Interestingly, both systems have a very similar viscosity of around 300−500 Pa·s at the onset of shear. Furthermore, recDgHBP-1 also exhibited shear-thinning behavior,[6] however, at a greater shear rate 0.3 s^{-1}.

Following the above considerations, we studied how droplets would interact with stiff networks of cellulose fibrils. In Figure 4B, it can be seen how droplets of LLC easily stick to cellulose fibers and infiltrate networks of these. The LLC droplets easily penetrated networks and filled space in-between fibers. Individual droplets showed stickiness to cellulose fibers.

We next studied how the silk inspired protein functioned as an adhesive, as it showed properties expected to be beneficial,

DOI: 10.1021/acsmacrolett.8b00527
ACS Macro Lett. 2018, 7, 1120−1125

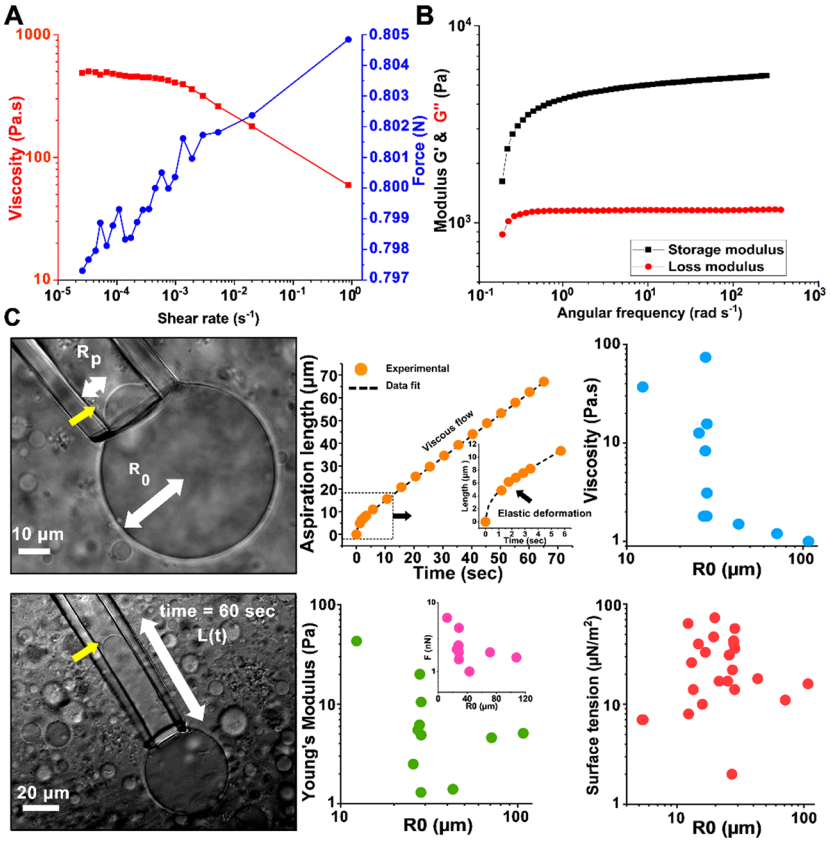

Figure 3. Properties of bulk and individual LLC droplets. (A) Viscosity of 30% w/v protein solution containing LLC droplets as the function of shear rate, showing shear-thinning (red squares show viscosity and blue circles force). (B) Shear-induced gelation during oscillatory viscosity measurement (G': storage modulus (black squares) and G'': loss modulus (red circles)). (C) Phase contrast images of an individual LLC droplet during micropipette aspiration experiment. Plots show an aspiration curve and the calculated interfacial energy, Young's modulus, and viscosity as a function of droplet size.

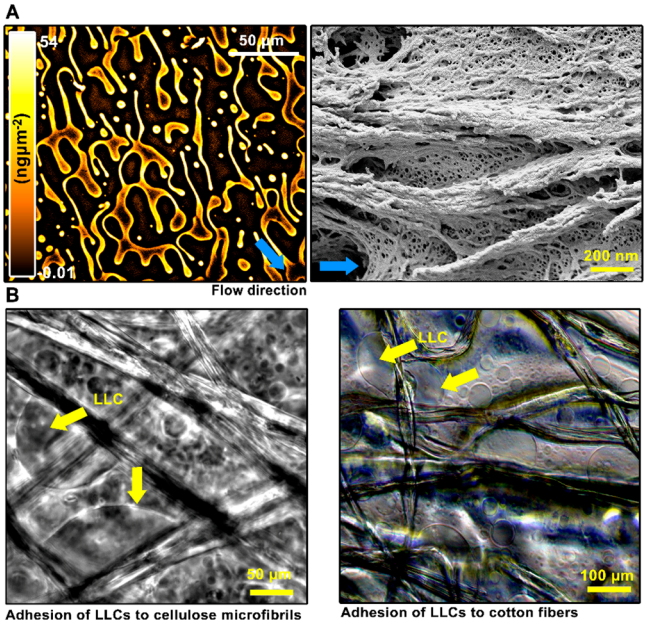

Figure 4. Fluid behavior of LLC and infiltration of cellulose fiber networks. (A) SLIM image of LLC deformation under shear. High-resolution cryo-fractured SEM image showing the deformation of the internal bicontinuous structure under shear. The blue arrow indicates direction of shear flow. (B) Infiltration and adhesion of LLC droplets (indicated with yellow arrows) on the surface and at the junctions of cotton fibers.

such as low surface energy, high protein concentration, high infiltration capability, and intermolecular interactions (Figure 1F). The CBM-eADF3-CBM interactions are evident even in conditions where the sample has been dried, as shown by breaking a sample of dried on a surface[12] (Figure S10). The protein forms long fibers that span the cracks that formed during breakage, demonstrating a possible cohesive mechanism similar to that known as necking in polymer science.[22] Figure 5A displays the bond strength of coacervated CBM-eADF3-CBM at 30% w/v that was used to adhere different cellulosic materials such as nanofibrillated cellulose of both bacterial and plant origin, cotton, office paper, and wood. After application, samples were allowed to solidify and cure at ambient conditions after water evaporation (Figure S11). Bond strengths varied between 15 and 75 Ncm^{-2}, depending on the type of cellulosic substrate. This suggested an influence of inherent nano- and microstructured features on the bond strength, also possibly reflecting differences in pore size and surface properties of the different celluloses. Of all samples, bacterial cellulose had the highest bond strength. Decreasing the mass of the adhesive solution showed a substantial decrease in the bonding strength (Figure S12A). Controls made with different variations of blocks or the unrelated bovine serum albumin (BSA; Figures 5B and S12B) showed lower strength but also a much lower work of fracture, corresponding to the area under the fracture curve. SEM of the fractured surface of the specimens after tensile measurement test reviled that almost in all the cases debonding occurred due to structural failure of the bulk material, not the adhesive

DOI: 10.1021/acsmacrolett.8b00527
ACS Macro Lett. 2018, 7, 1120−1125

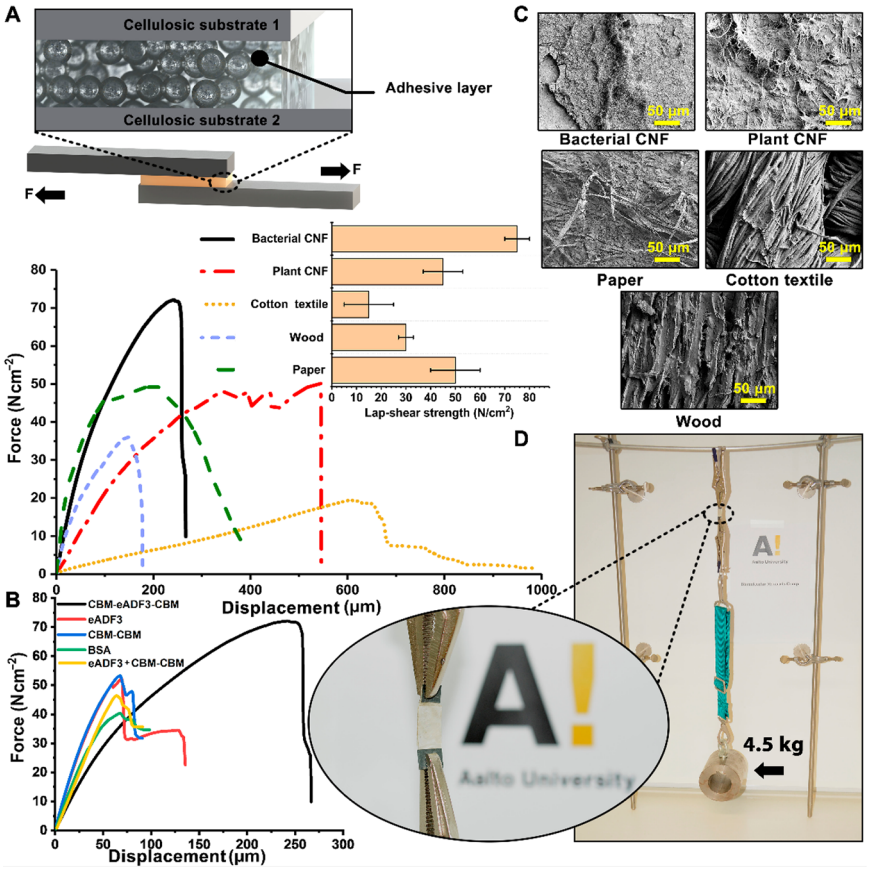

Figure 5. Bond strength of the coacervated CBM-eADF3-CBM. (A) Representative lap-shear strength curve for various cellulosic material. Column plot shows calculated the mean and standard deviation of the lap-shear strength (N = 5). (B) Representative lap-shear strength curves of bacterial cellulose glued by CBM-eADF3-CBM (black), eADF3 (red), CBM-CBM (blue), a mixture of eADF3 and CBM-CBM (yellow), and bovine serum albumin (BSA) (green). (C) SEM micrographs from the surface of debonded specimens for the corresponding specimens after tensile measurement. (D) Illustrating the adhesive strength of the LLC by hanging a 4.5 kg weight from two pieces of glued bacterial cellulose mat.

(Figures 5C and S13), suggesting that the adhesive formed a very strong interfacial bond (Figure 5D and Videos 6 and 7) to the cellulosic surfaces. However, debonding of the wood and cotton textile happened cohesively, and left adhesive on both surfaces illustrating that cracks propagated through the adhesive.

In summary, protein condensates should be seen as an essential aspect of polymer behavior for proteins and represent a key step for understanding when expanding the use of proteins for new uses such as adhesives. By using highly accurate methods of in situ protein concentration measurements, diffusivity measurements, and rheology of individual droplets, we found that the droplets showed a range of properties indicating that they are thermodynamically metastable, with varying properties between individual drops. Overall, the protein showed unique phase behavior and molecular structuring into highly deformable and low-interfacial energy assemblies. We showed how the preassemblies of the highly concentrated droplet in combination with low interfacial energy and cohesiveness could be efficiently employed as an intermediate state for strong adhesive assembly between cellulosic surfaces.

■ ASSOCIATED CONTENT

Supporting Information

The Supporting Information is available free of charge on the ACS Publications website at DOI: 10.1021/acsmacrolett.8b00527.

Details for all the materials and experimental methods (PDF).

Video 1: Formation and growth of multiple LLC droplets in water (AVI).

Video 2: Formation and growth of single LLC droplet in water (AVI).

Video 3: Coalescence of three individual LLC droplets, all varying in size and protein content, results in the expansion and increase of the protein content after each fusion (AVI).

Video 4: Fluorescent recovery after photobleaching part of the LLC droplet that was used to calculated diffusion coefficient of CBM-eADF3-CBM molecules (AVI).

Video 5: Micropipette aspiration of a LLC droplet (AVI).

Video 6: Illustrating deformation of LLC droplet into fluid threads under shear forces (AVI).

Video 7: Illustrating adhesive behavior of the LLC solution by gluing two pieces of normal paper to each other (AVI).

■ AUTHOR INFORMATION

Corresponding Authors

*E-mail: pezhman.mohammadi@aalto.fi.

*E-mail: markus.linder@aalto.fi.

ORCID

Pezhman Mohammadi: 0000-0003-4593-5371

Markus B. Linder: 0000-0002-7271-6441

DOI: 10.1021/acsmacrolett.8b00527
ACS Macro Lett. 2018, 7, 1120−1125

Notes

The authors declare no competing financial interest.

■ ACKNOWLEDGMENTS

We would like to thank Aalto University Nanomicroscopy Center (Espoo), Helsinki University Light-Microscopy Unit (Helsinki). The work was performed within the Academy of Finland Center of Excellence Programme (2014−2019) and Academy of Finland Projects 264493, 317019, and 307474, and COST Action CA15216.

■ REFERENCES

(1) Banani, S. F.; Lee, H. O.; Hyman, A. A.; Rosen, M. K. Biomolecular Condensates: Organizers of Cellular Biochemistry. *Nat. Rev. Mol. Cell Biol.* **2017**, *18*, 285.

(2) Mitrea, D. M.; Kriwacki, R. W. Phase Separation in Biology; Functional Organization of a Higher Order. *Cell Commun. Signaling* **2016**, *14* (1), na.

(3) Waite, J. H. Mussel Adhesion − Essential Footwork. *J. Exp. Biol.* **2017**, *220* (4), 517−530.

(4) Bahn, S. Y.; Jo, B. H.; Choi, Y. S.; Cha, H. J. Control of Nacre Biomineralization by Pif80 in Pearl Oyster. *Sci. Adv.* **2017**, *3* (8), e1700765.

(5) Weber, S. C.; Brangwynne, C. P. Getting RNA and Protein in Phase. *Cell* **2012**, *149* (6), 1188−1191.

(6) Tan, Y.; Hoon, S.; Guerette, P. A.; Wei, W.; Ghadban, A.; Hao, C.; Miserez, A.; Waite, J. H. Infiltration of Chitin by Protein Coacervates Defines the Squid Beak Mechanical Gradient. *Nat. Chem. Biol.* **2015**, *11* (7), 488−495.

(7) Wei, W.; Tan, Y.; Martinez Rodriguez, N. R.; Yu, J.; Israelachvili, J. N.; Waite, J. H. A Mussel-Derived One Component Adhesive Coacervate. *Acta Biomater.* **2014**, *10* (4), 1663−1670.

(8) Stewart, R. J.; Wang, C. S.; Song, I. T.; Jones, J. P. The Role of Coacervation and Phase Transitions in the Sandcastle Worm Adhesive System. *Adv. Colloid Interface Sci.* **2017**, *239*, 88−96.

(9) Wei, W.; Petrone, L.; Tan, Y.; Cai, H.; Israelachvili, J. N.; Miserez, A.; Waite, J. H. An Underwater Surface-Drying Peptide Inspired by a Mussel Adhesive Protein. *Adv. Funct. Mater.* **2016**, *26* (20), 3496−3507.

(10) Cai, H.; Gabryelczyk, B.; Manimekalai, M. S. S.; Grüber, G.; Salentinig, S.; Miserez, A. Self-Coacervation of Modular Squid Beak Proteins − a Comparative Study. *Soft Matter* **2017**, *13*, 7740−7752.

(11) Kontturi, E.; Laaksonen, P.; Linder, M. B.; Nonappa, A. H.; Gröschel, A. H.; Rojas, O. J.; Ikkala, O. Advanced Materials through Assembly of Nanocelluloses. *Adv. Mater.* **2018**, *30*, 1703779.

(12) Mohammadi, P.; Aranko, A. S.; Lemetti, L.; Cenev, Z.; Zhou, Q.; Virtanen, S.; Landowski, C. P.; Penttilä, M.; Fischer, W. J.; Wagermaier, W.; et al. Phase Transitions as Intermediate Steps in the Formation of Molecularly Engineered Protein Fibers. *Commun. Biol.* **2018**, *1* (1), 86.

(13) Eisoldt, L.; Thamm, C.; Scheibel, T. The Role of Terminal Domains during Storage and Assembly of Spider Silk Proteins. *Biopolymers* **2012**, *97* (6), 355−361.

(14) Huemmerich, D.; Helsen, C. W.; Quedzuweit, S.; Oschmann, J.; Oschmann, J.; Rudolph, R.; Scheibel, T. Primary Structure Elements of Spider Dragline Silks and Their Contribution to Protein Solubility. *Biochemistry* **2004**, *43* (42), 13604−13612.

(15) Guerette, P. a.; Ginzinger, D. G.; Weber, B. H.; Gosline, J. M. Silk Properties Determined by Gland-Specific Expression of a Spider Fibroin Gene Family. *Science* **1996**, *272* (5258), 112−115.

(16) Gosline, J. M.; Guerette, P. a.; Ortlepp, C. S.; Savage, K. N. The Mechanical Design of Spider Silks: From Fibroin Sequence to Mechanical Function. *J. Exp. Biol.* **1999**, *202* (23), 3295−3303.

(17) Gasteiger, E.; Hoogland, C.; Gattiker, A.; Duvaud, S.; Wilkins, M.; Appel, R.; Bairoch, A. Protein Identification and Analysis Tools on the ExPASy Server. In *The Proteomics Protocols Handbook*; Walker, J., Ed.; Humana Press, 2005; pp 571−607.

(18) Dosztányi, Z.; Csizmok, V.; Tompa, P.; Simon, I. IUPred: Web Server for the Prediction of Intrinsically Unstructured Regions of Proteins Based on Estimated Energy Content. *Bioinformatics* **2005**, *21* (16), 3433−3434.

(19) Tormo, J.; Lamed, R.; Chirino, A. J.; Morag, E.; Bayer, E. A.; Shoham, Y.; Steitz, T. A. Crystal Structure of a Bacterial Family-III Cellulose-Binding Domain: A General Mechanism for Attachment to Cellulose. *EMBO J.* **1996**, *15* (21), 5739.

(20) Hedhammar, M.; Rising, A.; Grip, S.; Martinez, A. S.; Nordling, K.; Casals, C.; Stark, M.; Johansson, J. Structural Properties of Recombinant Nonrepetitive and Repetitive Parts of Major Ampullate Spidroin 1 from Euprosthenops Australis: Implications for Fiber Formation. *Biochemistry* **2008**, *47* (11), 3407−3417.

(21) Mir, M.; Wang, Z.; Shen, Z.; Bednarz, M.; Bashir, R.; Golding, I.; Prasanth, S. G.; Popescu, G. Optical Measurement of Cycle-Dependent Cell Growth. *Proc. Natl. Acad. Sci. U. S. A.* **2011**, *108* (32), 13124−13129.

(22) Leonov, A. I. A. Theory of Necking in Semi-Crystalline Polymers. *Int. J. Solids Struct.* **2002**, *39* (24), 5913−5926.

DOI: 10.1021/acsmacrolett.8b00527
ACS Macro Lett. 2018, 7, 1120−1125